

Changes in rotational characters of one- and two-phonon γ -vibrational bands in ^{105}Mo

Masayuki Matsuzaki*

*Department of Physics, Fukuoka University of Education,
Munakata, Fukuoka 811-4192, Japan*

(Dated: December 22, 2014)

Abstract

The γ vibration is the most typical low-lying collective motion prevailing the nuclear chart. But only few one-phonon rotational bands in odd- A nuclei have been known. Furthermore, two-phonon states, even the band head, have been observed in a very limited number of nuclides not only of odd- A but even-even. Among them, that in ^{105}Mo is unique in that Coriolis effects are expected to be stronger than in ^{103}Nb and ^{105}Nb on which theoretical studies were reported. Then the purpose of the present work is to study ^{105}Mo paying attention to rotational character change of the one-phonon and two-phonon bands. The particle-vibration coupling model based on the cranking model and the random-phase approximation is used to calculate the vibrational states in rotating odd- A nuclei. The present model reproduces the observed yrast zero-phonon and one-phonon bands well. Emerging general features of the rotational character change from low spin to high spin are elucidated. In particular, the reason why the one-phonon band does not exhibit signature splitting is clarified. The calculated collectivity of the two-phonon states, however, is located higher than observed.

PACS numbers: 21.10.Re, 21.60.Jz, 27.60.+j

*matsuza@fukuoka-edu.ac.jp

I. INTRODUCTION

Based on the long history of physics of the atomic nucleus as a finite quantum many-body system bound by the strong interaction, nowadays, on the one hand interactions between two, or among three or more, nucleons can be related to quantum chromodynamics and the interaction thus obtained can be used as an input to large-scale shell-model calculations. On the other hand, from the mean-field picture, density-functional theories that describe ground states of nuclides of wide range in the nuclear chart are developing. For a class of excited states, the generator-coordinate method is used. Applications of such a framework to light odd- A nuclei are just begun [1].

Aside from these progresses, traditional effective models are still indispensable to describe detailed properties of collective excitations. In finite many-body systems, individual particle motions and collective motions are of similar energy scales hence couple to each other. In addition, they are sensitive to the numbers of constituents or the shell filling. Collective vibrations are not necessarily harmonic oscillations and whether multiple excitations exist or not is not trivial.

One of the typical collective motions in medium-heavy nuclei is the γ vibration. But its double excitation has been known in a limited number of nuclides such as ^{168}Er [2], ^{166}Er [3, 4], ^{164}Dy [5], ^{232}Th [6], ^{106}Mo [7], ^{104}Mo [8], and ^{138}Nd [9] in even-even nuclei. Among them, ^{168}Er , firstly observed one, was studied in terms of various theoretical approaches as reviewed in Ref. [10].

In odd- A nuclei, the first observation of the two-phonon γ vibration was made in ^{105}Mo [11], on which any theoretical studies has not been reported to the author's knowledge, and to which the present study is devoted. Then similar excitations were observed in ^{103}Nb [12] and ^{107}Tc [13]. The first realistic calculation on ^{103}Nb [14] was performed in terms of the triaxial projected shell model. After that the present author made a calculation on this nuclide in terms of the particle-vibration coupling model in Ref. [10].

Quite recently, two-phonon states very similar to those in ^{103}Nb were observed in ^{105}Nb [15]. In these isotopes, candidates of three-phonon states that fed two-phonon bands strongly were also indicated. If their property is confirmed, they are the first three-phonon excitation in deformed nuclei, and may indicate that there is a mechanism that makes odd- A nuclei more favorable for realizing three-phonon γ vibrations than even-even nuclei, although

spectra of odd- A nuclei are thought to be more complex than those of even-even nuclei in general. The present author studied in Ref. [16] these three-phonon candidates with invoking a method to calculate interband $B(E2)$ s based on the generalized intensity relation [17]. The result is promising but still not definitive.

Returning to two-phonon states, the odd particle that couples to them in ^{103}Nb and ^{105}Nb is in the $\pi[422] 5/2^+$ orbital originating from the $g_{9/2}$ subshell on which Coriolis effects are not very strong. Then states at finite rotation still can be approximately classified in terms of K , the projection of the angular momentum to the z axis. In contrast, the odd particle in ^{105}Mo is in the $\nu[532] 5/2^-$ orbital originating from the $h_{11/2}$ subshell on which Coriolis effects are stronger. Accordingly character of rotational band members would be different. This point is the main concern of the present work.

Throughout this paper the $\hbar = 1$ unit is used.

II. THE MODEL AND PARAMETERS

The particle-vibration coupling (PVC) model based on the cranking model and the random-phase approximation (RPA) is used for calculating eigenstates of odd- A nuclei. In the first step, the one-dimensionally cranked Nilsson plus BCS one-body Hamiltonian is diagonalized,

$$\begin{aligned} h' &= h - \omega_{\text{rot}} J_x \\ &= \sum_{\mu} e'_{\mu} a_{\mu}^{\dagger} a_{\mu} + \sum_{\bar{\mu}} e'_{\bar{\mu}} a_{\bar{\mu}}^{\dagger} a_{\bar{\mu}} + \text{const}, \end{aligned} \quad (1)$$

where h is the standard Nilsson plus BCS Hamiltonian. This gives a set of quasiparticle (qp) states. Second, I apply the RPA to the residual two-body pairing plus doubly-stretched quadrupole-quadrupole interaction between qps,

$$\begin{aligned} H_{\text{int}} &= - \sum_{\tau=1,2} G_{\tau} \tilde{P}_{\tau}^{\dagger} \tilde{P}_{\tau} - \frac{1}{2} \sum_{K=0,1,2} \kappa_K^{(+)} Q_K''^{(+)\dagger} Q_K''^{(+)} - \frac{1}{2} \sum_{K=1,2} \kappa_K^{(-)} Q_K''^{(-)\dagger} Q_K''^{(-)} \\ &= \sum_n \omega_n X_n^{\dagger} X_n. \end{aligned} \quad (2)$$

This gives many RPA modes. Cranking and RPA calculations are done in the five major shells, $N_{\text{osc}} = 2 - 6$ for the neutron and $1 - 5$ for the proton. Among RPA modes, I choose the γ -vibrational phonons, $n = \gamma$ and $\bar{\gamma}$, with signature $r = \exp(-i\pi\alpha) = 1$ and -1 ,

respectively, which have outstandingly large $K = 2$ transition amplitudes. Regarding them as elementary excitations, I diagonalize the PVC Hamiltonian,

$$\begin{aligned}
H_{\text{couple}}(\gamma) = & \sum_{\mu\nu} \Lambda_{\gamma}(\mu\nu) (X_{\gamma}^{\dagger} a_{\mu}^{\dagger} a_{\nu} + X_{\gamma} a_{\nu}^{\dagger} a_{\mu}) \\
& + \sum_{\mu\bar{\nu}} \Lambda_{\bar{\gamma}}(\mu\bar{\nu}) (X_{\bar{\gamma}}^{\dagger} a_{\mu}^{\dagger} a_{\bar{\nu}} + X_{\bar{\gamma}} a_{\bar{\nu}}^{\dagger} a_{\mu}) \\
& + \text{sig. conj.}
\end{aligned} \tag{3}$$

These calculations are performed in terms of signature-classified bases, and all the resulting quantities are given as continuous functions of the rotational frequency ω_{rot} . Detailed expressions of these formulations were given in Ref. [10].

Diagonalizations of the PVC Hamiltonian are performed in the model space spanned by $0 - 4\gamma$ basis states as in Ref. [16]. Here $n\gamma$ basis states designate $1\text{qp} \otimes (\gamma \text{ or } \bar{\gamma})^n$ states. Because there are two types of γ -vibrational phonons, γ and $\bar{\gamma}$, $(1\text{qp})_{r=\pm i} \otimes \gamma$ and $(1\text{qp})_{r=\mp i} \otimes \bar{\gamma}$ are possible for the 1γ states in the $r = \pm i$ sector. Similarly, there are 3 - 5 types of $2 - 4\gamma$ basis states, respectively, for each signature. The concrete form of eigenstates with $r = -i$ was given by Eq. (7) in Ref. [16]. That with $r = +i$, obtained by interchanging μ and $\bar{\mu}$, is given here.

$$\begin{aligned}
|\bar{\chi}_i\rangle = & \sum_{\bar{\mu}} \psi_i^{(1)}(\bar{\mu}) a_{\bar{\mu}}^{\dagger} |\phi\rangle \\
& + \sum_{\bar{\mu}} \psi_i^{(3)}(\bar{\mu}\gamma) a_{\bar{\mu}}^{\dagger} X_{\gamma}^{\dagger} |\phi\rangle + \sum_{\mu} \psi_i^{(3)}(\mu\bar{\gamma}) a_{\mu}^{\dagger} X_{\bar{\gamma}}^{\dagger} |\phi\rangle \\
& + \sum_{\bar{\mu}} \psi_i^{(5)}(\bar{\mu}\gamma\gamma) \frac{1}{\sqrt{2}} a_{\bar{\mu}}^{\dagger} (X_{\gamma}^{\dagger})^2 |\phi\rangle + \sum_{\bar{\mu}} \psi_i^{(5)}(\bar{\mu}\bar{\gamma}\bar{\gamma}) \frac{1}{\sqrt{2}} a_{\bar{\mu}}^{\dagger} (X_{\bar{\gamma}}^{\dagger})^2 |\phi\rangle \\
& + \sum_{\mu} \psi_i^{(5)}(\mu\gamma\bar{\gamma}) a_{\mu}^{\dagger} X_{\gamma}^{\dagger} X_{\bar{\gamma}}^{\dagger} |\phi\rangle \\
& + \sum_{\bar{\mu}} \psi_i^{(7)}(\bar{\mu}\gamma\gamma\gamma) \frac{1}{\sqrt{3!}} a_{\bar{\mu}}^{\dagger} (X_{\gamma}^{\dagger})^3 |\phi\rangle + \sum_{\mu} \psi_i^{(7)}(\mu\bar{\gamma}\bar{\gamma}\bar{\gamma}) \frac{1}{\sqrt{3!}} a_{\mu}^{\dagger} (X_{\bar{\gamma}}^{\dagger})^3 |\phi\rangle \\
& + \sum_{\mu} \psi_i^{(7)}(\mu\gamma\gamma\bar{\gamma}) \frac{1}{\sqrt{2}} a_{\mu}^{\dagger} (X_{\gamma}^{\dagger})^2 X_{\bar{\gamma}}^{\dagger} |\phi\rangle + \sum_{\bar{\mu}} \psi_i^{(7)}(\bar{\mu}\gamma\bar{\gamma}\bar{\gamma}) \frac{1}{\sqrt{2}} a_{\bar{\mu}}^{\dagger} X_{\gamma}^{\dagger} (X_{\bar{\gamma}}^{\dagger})^2 |\phi\rangle \\
& + \sum_{\bar{\mu}} \psi_i^{(9)}(\bar{\mu}\gamma\gamma\gamma\gamma) \frac{1}{\sqrt{4!}} a_{\bar{\mu}}^{\dagger} (X_{\gamma}^{\dagger})^4 |\phi\rangle + \sum_{\bar{\mu}} \psi_i^{(9)}(\bar{\mu}\bar{\gamma}\bar{\gamma}\bar{\gamma}\bar{\gamma}) \frac{1}{\sqrt{4!}} a_{\bar{\mu}}^{\dagger} (X_{\bar{\gamma}}^{\dagger})^4 |\phi\rangle \\
& + \sum_{\mu} \psi_i^{(9)}(\mu\gamma\gamma\gamma\bar{\gamma}) \frac{1}{\sqrt{3!}} a_{\mu}^{\dagger} (X_{\gamma}^{\dagger})^3 X_{\bar{\gamma}}^{\dagger} |\phi\rangle + \sum_{\mu} \psi_i^{(9)}(\mu\gamma\bar{\gamma}\bar{\gamma}\bar{\gamma}) \frac{1}{\sqrt{3!}} a_{\mu}^{\dagger} X_{\gamma}^{\dagger} (X_{\bar{\gamma}}^{\dagger})^3 |\phi\rangle \\
& + \sum_{\bar{\mu}} \psi_i^{(9)}(\bar{\mu}\gamma\gamma\bar{\gamma}\bar{\gamma}) \frac{1}{2} a_{\bar{\mu}}^{\dagger} (X_{\gamma}^{\dagger})^2 (X_{\bar{\gamma}}^{\dagger})^2 |\phi\rangle.
\end{aligned} \tag{4}$$

In the present work, μ and $\bar{\mu}$ run 21 states in the neutron $N_{\text{osc}} = 5$ shell.

The bands in ^{105}Mo studied in the present work are the yrast $\nu[532] 5/2^-$ band and corresponding single- and double- γ -vibrational bands. In the following, qp states at finite γ and ω_{rot} are also designated by the dominant asymptotic states. The lowest qp states with the dominant $\nu[532] 5/2^-$ component are denoted by $\bar{\mu} = \bar{1}$ and $\mu = 1$ for $r = +i$ and $r = -i$, respectively. These are the dominant components of the lowest (zero-phonon) PVC eigenstate in each signature. Then the two dominant components of the one-phonon PVC eigenstates are $\bar{1} \otimes \gamma$ and $1 \otimes \bar{\gamma}$ for $r = +i$ while $1 \otimes \gamma$ and $\bar{1} \otimes \bar{\gamma}$ for $r = -i$. Straightforwardly, those of the two-phonon in $r = +i$ are $\bar{1} \otimes \gamma\gamma$, $\bar{1} \otimes \bar{\gamma}\bar{\gamma}$, and $1 \otimes \gamma\bar{\gamma}$, while those in $r = -i$ are $1 \otimes \gamma\gamma$, $1 \otimes \bar{\gamma}\bar{\gamma}$, and $\bar{1} \otimes \gamma\bar{\gamma}$. The sum of the fractions of these main components defines the collectivity of calculated eigenstates.

The parameters entering into the calculation are chosen in a manner similar to the case of Refs. [10] and [16]. Concretely, the pairing gaps, $\Delta_n = 1.05$ MeV and $\Delta_p = 0.85$ MeV, are those widely used for both even- and odd- A nuclides in this mass region [7, 12]. The quadrupole deformation, $\epsilon_2 = 0.3254$, is the same as that adopted for the isobar ^{105}Nb in Ref. [16]. The triaxial deformation γ is chosen so that the calculated signature splitting $\Delta e'$ between the lowest PVC eigenstates reproduces overall features of the observed one. The resulting value, $\gamma = -10^\circ$, is again the same as that for ^{105}Nb . For the quadrupole interaction strengths, examined in the first attempt were those which reproduce the observed γ -vibrational energy ω_γ , 0.8121 MeV of ^{104}Mo [8] or 0.7104 MeV of ^{106}Mo [7] or their average, in the RPA calculation for the even-even core state at each γ as in previous calculations [10, 16, 18, 19]. But these were unsuccessful because there exists the $\nu[541] 3/2^-$ qp-dominant state slightly higher than the one-phonon states in the PVC calculation and the former pushes down the latter. This contradicts the observed situation that the γ -vibrational energy of ^{105}Mo is higher than those of ^{104}Mo and ^{106}Mo , see Fig. 10 of Ref. [11]. To reproduce this phenomenologically, adopted are the interaction strengths that give $\omega_\gamma = 1.0$ MeV in the RPA calculation for the even-even core and consequently bring the one-phonon states higher than the $\nu[541] 3/2^-$ -dominant state in the PVC calculation at $\omega_{\text{rot}} = 0$. After rotation sets in, calculated ω_γ and $\omega_{\bar{\gamma}}$ in the RPA calculation almost degenerate up to $\omega_{\text{rot}} = 0.3$ MeV, then at this rotational frequency, the γ with $r = +1$ is crossed by the steeply down-slope $(\nu[532] 5/2^-)^2$ state. This crossing produces irregularities in the PVC calculation. The configuration with this aligned is the s -band state in this mass region and would become the

yrast in the even-even core when its Routhian reaches 0 at higher ω_{rot} although this crossing is blocked in the odd- A system with one of the $\nu[532] 5/2^-$ signature-partner pair is already occupied. Therefore irregularities at $\omega_{\text{rot}} = 0.3$ MeV are artifacts of the model and should be ignored. After this crossing, ω_γ is slightly larger than $\omega_{\bar{\gamma}}$.

III. RESULTS AND DISCUSSION

The Routhians in the one-phonon region are shown in Figs. 1 (a) for $r = +i$ and (b) for $r = -i$. There are three eigenstates around $e' = 1.8$ MeV at $\omega_{\text{rot}} \sim 0$ in both signature sectors. If the static triaxial deformation that mixes the K quantum number is ignored, the second, third, and fourth states are the $\nu[541] 3/2^-$, the $K = \Omega - 2 = 1/2$ γ vibration, and the $K = \Omega + 2 = 9/2$ γ vibration, respectively, hereafter j and Ω are the single-particle angular momentum and its projection to the z axis.

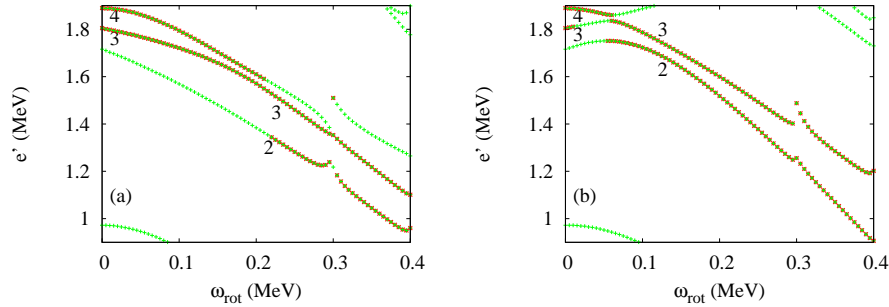


FIG. 1: (Color online) Routhians of all calculated PVC states in the region of one-phonon bands are shown by green +s, (a) in the $r = +i$ sector and (b) in the $r = -i$ sector. Those with more than 50% collective fraction are emphasized by red x's. The labels attached designate the numbers, i in Eq. (4) in the present article for $r = +i$ and in Eq. (7) in Ref. [16] for $-i$, enumerated from the lowest. Note that the lowest state seen only in small ω_{rot} in each figure is the yrast zero-phonon state.

In the single- j approximation effective for high- j cases, the favored state ($r = +i$ in the present case) is written as $|f_\Omega\rangle = \frac{1}{\sqrt{2}}(|\Omega\rangle + |-\Omega\rangle)$ while the unfavored state ($r = -i$ in the present case) is $|u_\Omega\rangle = \frac{1}{\sqrt{2}}(|\Omega\rangle - |-\Omega\rangle)$ at $\omega_{\text{rot}} = 0$ aside from overall phases. Therefore those with $\Omega = 1/2$ have diagonal matrix elements of J_x and consequently their Routhians, eigenvalues of $h' = h - \omega_{\text{rot}} J_x$, split as soon as rotation sets in. This splitting propagates to

other states through the Ω mixing at finite ω_{rot} . This is the basic mechanism of the signature splitting. In addition, when triaxial deformation, represented by the term proportional to $Q_2^{(+)} = \frac{1}{\sqrt{2}}(Q_{22} + Q_{2-2})$ in h , and/or couplings to the γ vibration exist, $\Omega = 3/2$ states also split through $\langle 3/2|Q_{22}| - 1/2\rangle \times \langle -1/2|J_x|1/2\rangle \times \langle 1/2|Q_{22}| - 3/2\rangle$, for example. This is the reason why both the noncollective second and the collective third states exhibit finite alignments $= -de'/d\omega_{\text{rot}}$ at $\omega_{\text{rot}} = 0$ and interact with each other at finite ω_{rot} . Because the mutual repulsion extends over wide range of ω_{rot} , the third (originally lower one-phonon) state is pushed up and interacts also with the fourth (originally upper one-phonon) state. Then at $\omega_{\text{rot}} > 0.2$ MeV the third state carries the character of the upper one-phonon state in $r = +i$ whereas the effect of the noncollective state is only local in $r = -i$.

Aside from this perturbation from the noncollective state, the collective states show the pattern, common to the previous cases of ^{103}Nb and ^{105}Nb , that the lower one-phonon state has $K = \Omega - 2$ with a finite alignment (positive for the favored and negative for the unfavored) and the upper one has $K = \Omega + 2$ with negligible alignment for small ω_{rot} , see Fig. 3(a) in Ref. [16]. For example, in the $r = -i$ sector, both of them are dominantly composed of the $1 \otimes \gamma$ and the $\bar{1} \otimes \bar{\gamma}$ basis states. Two orthogonal combinations of them with similar magnitudes form the eigenstates with $K = \Omega - 2$ and $\Omega + 2$ as discussed in Ref. [16]. This pattern is preserved in the whole calculated range of ω_{rot} in the cases of ^{103}Nb and ^{105}Nb with the $\pi g_{9/2}$ odd particle with small signature splittings studied there.

In the present case of ^{105}Mo with the higher- j , $\nu h_{11/2}$, odd particle, in contrast, stronger Coriolis interactions change their characters as ω_{rot} increases. Actually slopes of their Routhians are as twice as those of ^{103}Nb and ^{105}Nb . Because the signature splitting between the 1 and the $\bar{1}$ basis states is significantly larger than that between γ and $\bar{\gamma}$, the $\bar{1} \otimes \bar{\gamma}$ component becomes dominant in the lower one-phonon state while the $1 \otimes \gamma$ component becomes dominant in the upper one in the $r = -i$ sector, for example.

This character change caused by the Coriolis K mixing can be clearly seen in the wave function shown in Fig. 2 for $r = -i$. Aside from the abrupt change brought about by the crossing with the noncollective state at around $\omega_{\text{rot}} = 0.06$ MeV, the $1 \otimes \gamma$ component becomes dominant in the upper one-phonon state at high ω_{rot} . The schematic behavior of the collective states is depicted in Fig. 3. This figure clearly explains the reason why the observed one-phonon band does not exhibit signature splitting in contrast to the yrast zero-phonon band: The observed one-phonon band with the $K = \Omega + 2$ band head does not

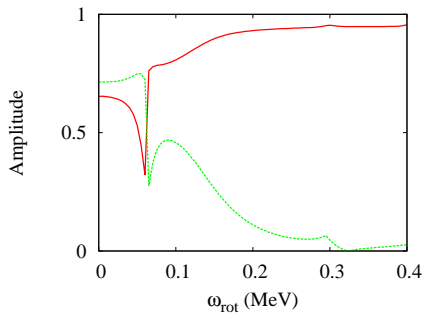


FIG. 2: (Color online) Amplitudes of the dominant components $|\psi_i^{(3)}(1\gamma)|$ (red solid) and $|\psi_i^{(3)}(\bar{1}\bar{\gamma})|$ (green dashed) in the upper ($i = 3$ at $\omega_{\text{rot}} > 0.06\text{MeV}$) one-phonon band in the $r = -i$ sector.

show signature splitting at $\omega_{\text{rot}} \sim 0$ because of the high K as argued in Ref. [16]. And at finite ω_{rot} , the $r = +i$ and $r = -i$ sequences of the band consist dominantly of the $1 \otimes \bar{\gamma}$ and $1 \otimes \gamma$, respectively, hence the splitting between them is essentially the difference $\omega_\gamma - \omega_{\bar{\gamma}}$, which is much smaller than the splitting in the yrast zero-phonon band. When the $r = -i$ is favored as in the $g_{9/2}$ and $i_{13/2}$ cases, 1 and $\bar{1}$ in the figure should be interchanged.

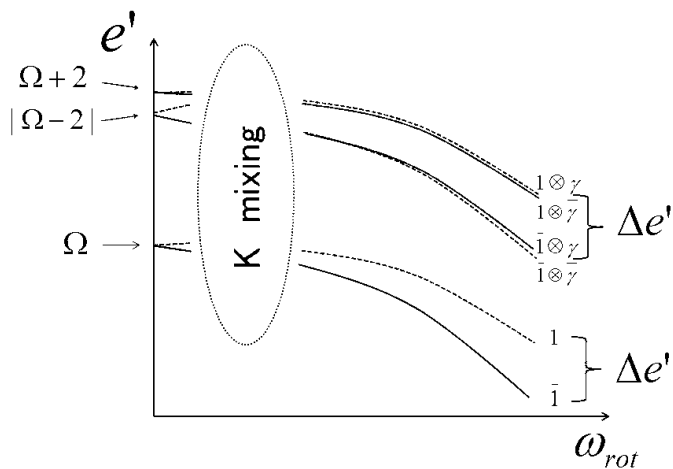


FIG. 3: Schematic drawing of the character change of the zero- and one-phonon bands from the K scheme to the signature scheme caused by the Coriolis K mixing.

The calculated zero- and one-phonon states are compared quantitatively with the observed ones. The reference rotating frame to which the data are converted is determined in two steps. First the Harris parameters are determined to fit the ground band up to 10^+ of

^{106}Mo as $\mathcal{J}_0 = 18.08 \text{ MeV}^{-1}$ and $\mathcal{J}_1 = 43.21 \text{ MeV}^{-3}$. In the second step the origin of this frame must be shifted in order to be compared with states in the odd- A system. Usually this overall shift is given by the pairing gap, in the present case $\Delta_n = 1.05 \text{ MeV}$, in the cranking calculation. In the present calculation, however, the cranking model is extended to the PVC model and this produces a downward shift of the Routhian of the lowest state, 0.078 MeV at $\omega_{\text{rot}} = 0$. Accordingly the overall shift is determined to be 0.972 MeV . The result is shown in Fig. 4. This shows that the zero- and one-phonon states are reproduced well.

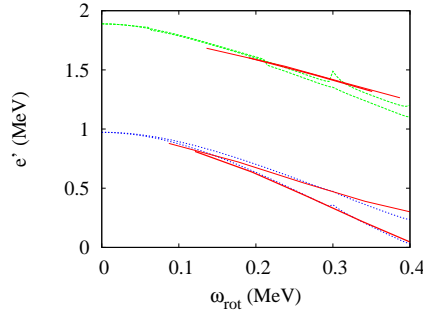


FIG. 4: (Color online) Routhians of calculated zero-phonon (blue dotted) and upper ($K = \Omega + 2$) one-phonon (green dashed) bands are compared with the corresponding data (red solid) converted to the rotating frame by using the Harris parameters $\mathcal{J}_0 = 18.08 \text{ MeV}^{-1}$ and $\mathcal{J}_1 = 43.21 \text{ MeV}^{-3}$ that fit the yrast band of ^{106}Mo [8]. Thick and thin curves designate the $r = +i$ and $-i$, respectively.

Now I proceed to the two-phonon states. How their calculated collectivity distributes is shown in Fig. 5 for $r = -i$ together with the zero- and one-phonon states at four ω_{rot} s. These figures show that the locations of the one-phonon and two-phonon states are harmonic at least their centers of the collective strength are seen. Experimentally, however, an anharmonicity, $E_{2\gamma}/E_{1\gamma} = 1.76$, was reported in contrast to the harmonic spectra in the adjacent even-even isotopes, ^{104}Mo [8] and ^{106}Mo [7]. Note here that an anharmonic $E_{2\gamma}$ in ^{106}Mo was cited in Ref. [11] referring to Ref. [20] but it is a misciting of the band-head energy of another band. Reference [20] reported the same harmonic value. These data suggest an unknown mechanism to produce anharmonicity proper to odd- A systems, different from the one discussed for even-even nuclei from a microscopic theoretical point of view in Ref. [22].

More closely, their Routhians are shown in Figs. 6 (a) for $r = +i$ and (b) for $r = -i$ as continuous functions of ω_{rot} . As in the cases of ^{103}Nb and ^{105}Nb , three sequences keep

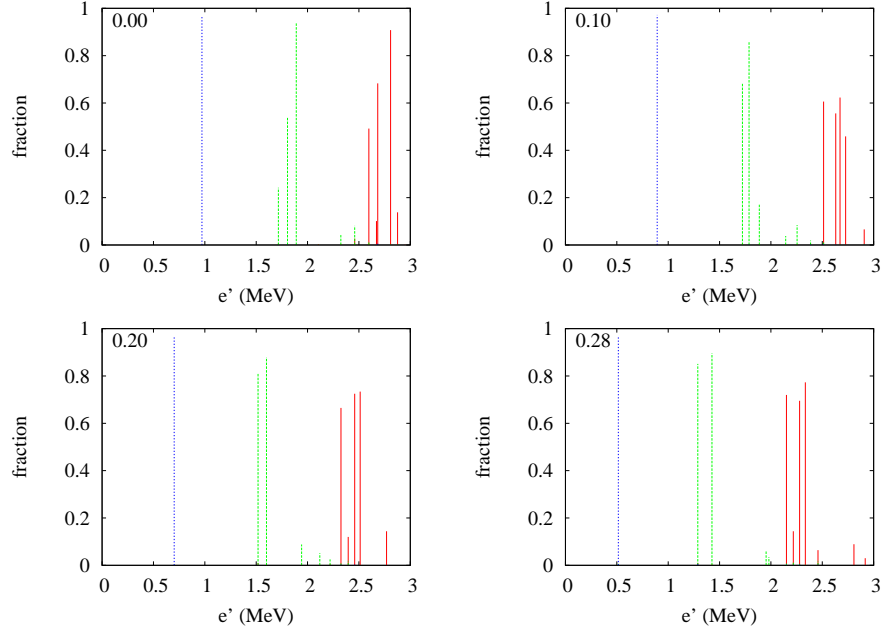


FIG. 5: (Color online) Distribution of the collective fraction (probability in the wave function) of the zero-, one-, and two-phonon components in the $r = -i$ sector, $|\psi^{(1)}(1)|^2$ (blue dotted), $|\psi^{(3)}(1\gamma)|^2 + |\psi^{(3)}(\bar{1}\bar{\gamma})|^2$ (green dashed), and $|\psi^{(5)}(1\gamma\gamma)|^2 + |\psi^{(5)}(1\bar{\gamma}\bar{\gamma})|^2 + |\psi^{(5)}(\bar{1}\gamma\bar{\gamma})|^2$ (red solid), respectively, at $\omega_{\text{rot}} = 0, 0.1, 0.2$, and 0.28 MeV.

collectivity in the whole calculated range of ω_{rot} although they are located in the region with larger level density. The lower one is of $K = |\Omega - 4| = 3/2$, the medium one is of $K = \Omega = 5/2$, and the upper one is of $K = \Omega + 4 = 13/2$ at $\omega_{\text{rot}} \sim 0$. Experimentally, the band head was assigned as $K = 13/2$ and only two states in each signature were observed. They are represented by a point in the Routhian diagram for each signature as indicated by red filled squares in Fig. 6.

The locations of the highest peaks of each phonon number in Fig. 5 for $\omega_{\text{rot}} = 0$ do not account for the observed anharmonicity at the band head. The calculated Routhians of the zero-phonon, (upper) one-phonon, and (upper) two-phonon states at $\omega_{\text{rot}} = 0$ are (1.050, 2.050, 3.050) MeV without PVC (not shown) while (0.972, 1.890, 2.808) MeV with PVC, respectively. However, at finite ω_{rot} where actual transitions are observed, the Coriolis effect is significant in the present high- j case and calculated states look in the signature scheme with mixed K . Inspection of the wave functions indicates that the dominant components are $\bar{1} \otimes \gamma\gamma$ for the lower, $\bar{1} \otimes \bar{\gamma}\bar{\gamma}$ for the medium, and $1 \otimes \gamma\bar{\gamma}$ for the upper in the $r = +i$ sector, while $\bar{1} \otimes \gamma\bar{\gamma}$ for the lower, $1 \otimes \bar{\gamma}\bar{\gamma}$ for the medium, and $1 \otimes \gamma\gamma$ for the upper in

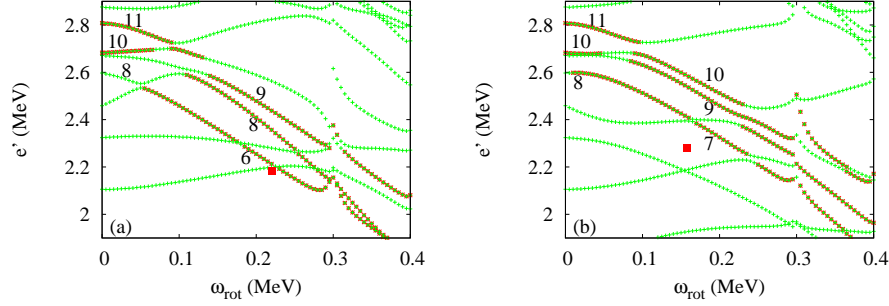


FIG. 6: (Color online) The same as Fig. 1 but in the region of two-phonon bands. Corresponding data (red filled square) converted to the rotating frame are also shown.

the $r = -i$ sector. Again this proves that the order of the collective states is ruled by the signature splitting between the 1 and $\bar{1}$ basis states as in the one-phonon states in Fig. 3. This indicates that their connection to the band head with fairly pure K is not trivial.

Then a natural criterion to choose the state to be identified with (the main component of) the observed one is the largest collectivity, as argued in the three-phonon-candidate cases in Ref. [16], because it is generally expected that the most collective sequence connected by strong $E2$ transitions would be observed. Actually the upper one, identified with the observed one at the band head, is the most collective at $\omega_{\text{rot}} = 0$ because its high- K property prevents it from mixing with other states. But three sequences become to share similar collectivities as soon as rotation sets in. As in the three-phonon case, the state with the highest K effectively has the highest j and accordingly feels the strongest Coriolis force as ω_{rot} increases. Then it is expected that band members that have large overlaps with the most collective eleventh state with the highest K at $\omega_{\text{rot}} \sim 0$ would be energetically lowered with reducing K as ω_{rot} increases and appear at lower Routhians through bandcrossing(s). The observed transitions are located near to ($r = +i$) or even lower than ($r = -i$) the lowest calculated two-phonon states. However, lowering of the location of collectivity to these lowest states in the present calculation is insufficient in contrast to the three-phonon case although j is larger. Therefore it is difficult to establish the mapping between them.

IV. CONCLUSIONS

To conclude, the yrast (zero-phonon) $\nu[532] 5/2^-$, the one- and two-phonon γ vibrational bands in ^{105}Mo have been calculated in the particle-vibration coupling model based on the

cranking model and the random-phase approximation paying attention to the rotational effects on the spectra in comparison to the lower- j cases of ^{103}Nb and ^{105}Nb studied in the previous works.

The zero- and one-phonon bands have been reproduced well. In particular, the rotational character change from the K scheme to the signature scheme through the Coriolis K mixing in the one-phonon states is stressed. This naturally accounts for the reason why the observed one-phonon band does not exhibit signature splitting in contrast to the yrast zero-phonon band. A specific feature of the data is that the two-phonon states show anharmonicity in the spectra that is absent in ^{103}Nb , ^{105}Nb , ^{104}Mo , and ^{106}Mo . This fact suggests that there exists an unknown mechanism to produce anharmonicity proper to high- j odd- A nuclei. The particle-vibration coupling pushes down them but the result is still harmonic with a slightly reduced interval at $\omega_{\text{rot}} = 0$. A possibility applicable to finite ω_{rot} , inspired from the previous calculation for the three-phonon-candidate states in ^{103}Nb and ^{105}Nb , is that the continuation of the highest-lying two-phonon state with the highest K would be energetically lowered by a strong Coriolis force. In the present calculation, however, its lowering is insufficient.

-
- [1] B. Bally, B. Avez, M. Bender, and P. -H. Heenen, Phys. Rev. Lett. **113**, 162501 (2014).
 - [2] W. F. Davidson et al., J. Phys. **G7**, 455; 843 (1981).
 - [3] C. Fahlander et al., Phys. Lett. **B388**, 475 (1996).
 - [4] P. E. Garrett et al., Phys. Rev. Lett. **78**, 4545 (1997).
 - [5] F. Corminboeuf et al., Phys. Rev. **C56**, R1201 (1997).
 - [6] W. Korten et al., Phys. Lett. **B317**, 19 (1993).
 - [7] A. Guessous et al., Phys. Rev. Lett. **75**, 2280 (1995).
 - [8] A. Guessous et al., Phys. Rev. **C53**, 1191 (1996).
 - [9] H. J. Li et al., Phys. Rev. **C87**, 057303 (2013).
 - [10] M. Matsuzaki, Phys. Rev. **C83**, 054320 (2011).
 - [11] H. B. Ding et al., Phys. Rev. **C74**, 054301 (2006).
 - [12] J. -G. Wang et al., Phys. Lett. **B675**, 420 (2009).
 - [13] L. Gu et al., Chin. Phys. Lett. **26**, 092502 (2009).
 - [14] J. A. Sheikh, G. H. Bhat, Y. Sun, and R. Palit, Phys. Lett. **B688**, 305 (2010).

- [15] H. J. Li et al., Phys. Rev. **C88**, 054311 (2013).
- [16] M. Matsuzaki, Phys. Rev. **C90**, 044313 (2014).
- [17] Y. R. Shimizu and T. Nakatsukasa, Nucl. Phys. **A611**, 22 (1996).
- [18] M. Matsuzaki, Y. R. Shimizu and K. Matsuyanagi, Prog. Theor. Phys. **77**, **1302** (1987); *ibid.* **79**, 836 (1988).
- [19] G. Gervais et al., Nucl. Phys. **A624**, 257 (1997).
- [20] R. Q. Xu et al., Chin. Phys. Lett. **19**, 180 (2002).
- [21] H. Hua et al., Phys. Rev. **C69**, 014317 (2004).
- [22] M. Matsuo and K. Matsuyanagi, Prog. Theor. Phys. **74**, 1227 (1985); *ibid.* **76**, 93 (1986); *ibid.* **78**, 591 (1987).